Design and Evaluation of Frequency Weighted LQG—Maximum Entropy Controllers on an Experimental Truss Structure

J. J. Allen

J. P. Lauffer

Sandia National Laboratories,
Albuquerque, NM 87185

This paper will discuss the experimental evaluation of a structural control system designed using a combination of Frequency Weighted LQG and Maximum Entropy. The experimental implementation was performed on an experimental truss structure, the Sandia Truss, which is described in the paper. The control design model was obtained via experimental system identification using the eigensystem realization algorithm with data correlation. The control design used frequency weighting to stabilize the unstructured uncertainty of the system due to low signal-to-noise and uncertain system dynamics in various frequency ranges. Maximum entropy is used to provide robustness for structured uncertain system dynamics within the controller bandwidth. The experimental implementation of the controllers designed with this approach show the ability to design controllers with a specified bandwidth, gain stabilization of unstructured uncertainty, and robustness to structured uncertainty within the controller bandwidth.

1 Introduction

Active control of structural vibrations is attaining increased importance in the design and proper operation of manufacturing as well as aerospace systems. The design of controllers for systems with significant structural flexibility presents a challenge because of the high order uncertain system dynamics and the multiple input/multiple output (MIMO) control laws required for some applications. There have been many optimal robust control methods (Maciejowski, 1989 and Hyland et al., 1993) developed for the design of MIMO robust control laws; however, there appears to be a significant gap between the theoretical development and experimental evaluation of control and identification methods to address structural control applications.

The linear quadratic gaussian (LQG) control method was developed thirty years ago and is capable of designing MIMO control laws. However, LQG controllers designed with white disturbance and sensor noises do not produce satisfactory results (Doyle, 1978), due to the infinite controller bandwidth and sensitivity to control model errors. Augmenting the model of the system dynamics with frequency weighting filters for the disturbance, sensor noise and control signal was proposed by Gupta (1980) to obtain a frequency weighted LQG (FWLQG) method. The FWLQG method can be used to design loopshaping controllers which gain stabilize unstructured system uncertainty. Safonov (1981) also suggested the use of colored noises in LQG design to obtain robustness in the control law. Opdenacker et al. (1990) describes the application of FWLQG to a one bay truss structure which had three dominant modes in the performance output and several less significant modes in the system dynamics, which was modeled for control design purposes by the finite element method. The experimental study in Opdenacker et al. (1990) produced stable but overly conservative control systems which limited the system performance.

Maximum Entropy (ME) is a method of modeling structured parameter uncertainty via a stochastic multiplicative white-noise process. This approach allows the performance/robustness trade-off to be determined by a quadratic cost function. Maximum Entropy specifically addresses real valued parameter uncertainties which are significant in the design of structural control systems. Maximum Entropy necessary conditions for optimality (Bernstein and Greeley, 1986) result in two Riccati and two Lyapunov equations which are coupled by the stochastic parameters. Solutions to the coupled Riccati and Lyapunov equations can be obtained by homotopy methods (Collins et al., 1994). Experimental evaluations of decentralized ME controllers are reported in Collins (1991 and 1992).

The purpose of this paper is to explore the use of Frequency Weighted LQG in conjunction with Maximum Entropy for the design of disturbance rejection controllers on an experimental truss structure. The frequency weighting will allow gain stabilization of the system dynamics in frequency ranges where there is unstructured uncertainty due to low signal to noise ratio (SNR) or high uncertainty in the system dynamics. Maximum entropy will be used for enhanced robustness of structured uncertainty due to uncertain system dynamics within the controller bandwidth.

The paper is organized as follows. Section 2 discusses the experimental truss structure and describes the control design problem. Section 3 discussed the experimental system identification which was performed to obtain a control design model for the system. Section 4 will present an overview of the control design methods used in this study; and, Section 5 will present the experimental control implementation results. Section 6 will summarize results and offer conclusions.

2 System Description and Control Design Requirements

To evaluate and demonstrate the effectiveness of the experimental system identification and robust control design techniques, we focused on an experimental program which utilized the Sandia Truss as a controlled structure test bed. The Sandia Truss is shown in Fig. 1, and, an instrumentation schematic is shown in Fig. 2. The truss is constructed from 1 in. diameter polycarbonate tubing bonded to polycarbonate blocks at the truss nodes. The truss is "Γ" shaped with five vertical bays

Contributed by the Dynamic Systems and Control Division for publication in the JOURNAL OF DYNAMIC SYSTEMS, MEASUREMENT, AND CONTROL. Manuscript received by the DSCD October 1994. Associate Technical Editor: N. Sadegh.

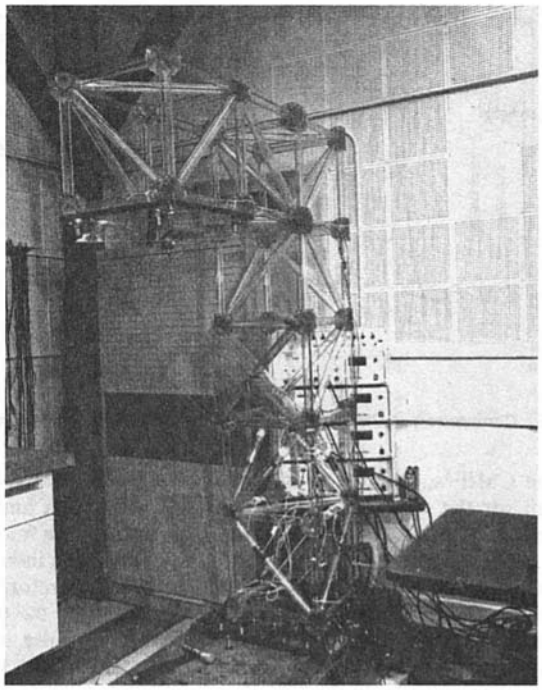

Fig. 1 The Sandia truss

providing the length and two horizontal bays at the top. Each bay is approximately one foot cube. Bolted to the surfaces of two bays are 0.5 in. polycarbonate plates stiffened with 0.5 in. thick ribs. The entire truss is cantilevered from a 2000 lbm seismic mass which in turn is supported on air bags to isolate the structure from high frequency base vibrations.

Eight feedback sensors are utilized to sense the axial strain in the diagonal struts of the bottom two bays of the truss. The sensors are made of polyvinyldene fluoride (PVDF) and are bonded directly to the tubes. These sensors are capable of detecting strains on the order of 10 nanostrain. Charge amplifiers are used as signal conditioners.

The feedback actuators are constructed out of a piezoelectric ceramic, lead magnesium niobate (PMN). The PMN actuators were fabricated in split rings to allow for the actuators to be applied after the construction of the truss. The PMN actuators apply an axial strain to the strut. They are driven by high gain/bandwidth amplifiers capable of providing the DC offset necessary for the PMN actuators. The use of wide bandwidth amplifiers is a major change from a previous study (Allen et al., 1990) in which the amplifier bandwidth extended to only 120 Hz. Four actuators are located on the diagonal members of the bottom bay of the truss.

The disturbance actuators are made out of PVDF and are identical to the feedback sensors. They are located on the axial struts of the second bay. Like the feedback actuators, the disturbance actuators apply axial strains to the struts.

The controllers were implemented by a digital controls processor. The processor is capable of implementing a 32 state controller with eight inputs and eight outputs while operating at a fixed sampling rate of 50 kHz. The effective transport delay across the processor, including zero order hold effects, is 35 μ seconds. To obtain the minimum delay, the processor implements a block-diagonal state-space form of the controller. The principle limitation of this digital processor is that it is incapable of directly implementing a controller in state space form which requires a through-put matrix. When required, the throughput matrix is approximated by including high-frequency real poles in the state transition matrix.

The performances minimized in this study were the x, y, z accelerations at the center of the plate on the top outboard bay. The performances are directly measured using high sensitivity piezoelectric accelerometers. The performances are used to evaluate the effectiveness of the controllers but are not used for control feedback.

The control design objective for this system can be stated as follows:

- Minimize the elastic response of the system at the performance locations (i.e., x, y, z response of the plate at the top outboard bay) in the frequency range of 10–120 Hz, while satisfying the following criteria:
  - Maintain system stability and performance in the face of high frequency uncertain or unmodelled dynamics.
  - Do not excite the low frequency suspension dynamics of the system ($<$10 Hz) whose dynamics are poorly characterized.

3 Experimental System Identification

Structural systems provide a significant challenge to system identification algorithms due to high order, high modal density, widely varying damping factors, and multiple inputs and outputs. Finite element models (FEM's) have a great difficulty producing models which are accurate beyond the first few global modes of the system, due to the modelling assumptions that must be made by the analyst, and the inability to apriori model some phenomena (i.e., joint stiffness and damping). Because of the added difficulty of updating FEM's, this study aimed at directly estimating analytical models from test data. The method used for estimating the dynamics of the system was the Eigensystem Realization Algorithm using Data Correlation (ERADC) (Juang, 1988), which extracts a model in a discrete state-space form.

For the system identification experiments, the first objective was to obtain input/output data from which a model could be extracted. ERADC operates on impulse response functions which were estimated by taking the inverse Fourier transforms of frequency response functions (FRF's). In estimating the FRF's, all eight actuators simultaneously excited the truss with uncorrelated burst random excitation. All of the actuator inputs and sensor response signals were simultaneously measured. FRF's were measured over the bandwidth of 0 to 200 Hz with a frequency resolution of 0.125 Hz/spectral line. No weighting windows were applied to the data. Additionally, a second FRF data set was acquired over the bandwidth of 0 to 25 Hz with a resolution of 0.0156 Hz/spectral line. Because of the presence of unmeasured external disturbances and the large number of inputs, an extremely high number of ensemble averages (200) were used in estimating the FRF's. The FRF's were calculated using the H_v estimator (Rocklin et al., 1985).

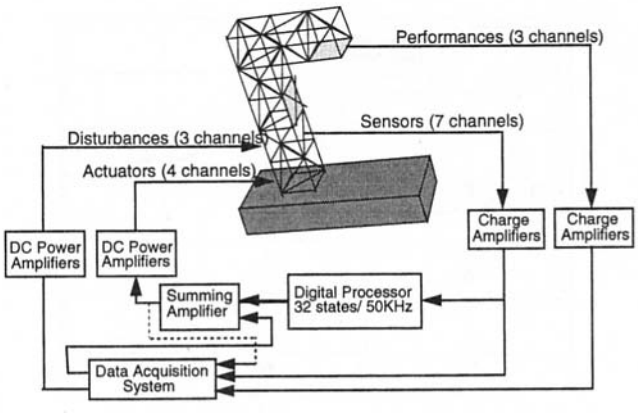

Fig. 2 Sandia truss instrumentation schematic

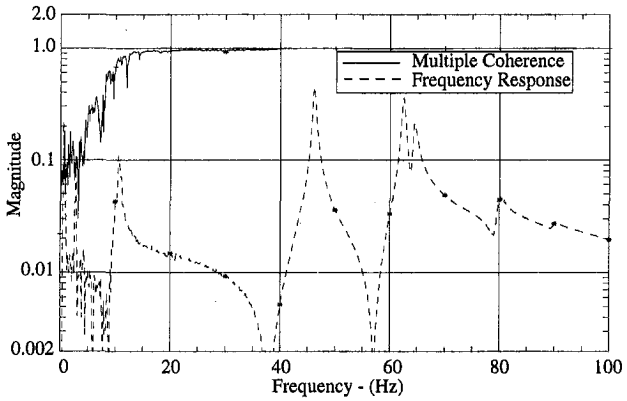

Fig. 3 FRF and multiple coherence function

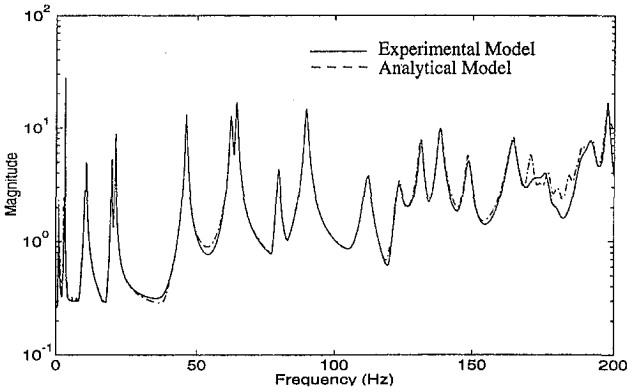

Fig. 5 Comparison of CMIF's from measured data and analytical model

In the course of estimating FRF's, we also estimated multiple coherence functions (Bendat and Piersol, 1986) and autospectra. These functions were useful in assessing the quality of the measured FRF's and determining the source of errors. Plotted in Fig. 3 are a FRF and a multiple coherence function. The FRF is noisy below 15 Hz, which corresponds to the low value of the multiple coherence function over this same frequency range. The noisy estimate of the FRF over this range is due to the low level of response of the structure due to the applied disturbances and the relatively high level response of the suspension modes due to unmeasured floor vibrations. This observation is further substantiated by comparing autospectra of one of the sensors with and without the artificial disturbance activated as shown in, Fig. 4. Below 15 Hz, the two autospectra have similar amplitudes which implies that most of the response over this band is due to the unmeasured disturbances.

Due to the noisy estimate of the FRF's over the low frequency band, the resultant models from any system identification technique would be substantially in error over this band. Because of the error in the model and the presence of unmeasured disturbances the low frequency range provides a challenge to the control design.

One of the challenges of employing system identification techniques like ERADC is estimating the order of the system. The principle approach is to select the order by observing the singular values of the system correlation matrix. Ideally, the correct order is determined from a sudden drop in the magnitude of the singular value plot. Unfortunately, because of the presence of nonlinearities, residual flexibilities, and marginally observable and controllable modes, the system order is seldom readily apparent. The main tool used for order determination in this study was the complex mode indicator function (CMIF) (Shih et al., 1989).

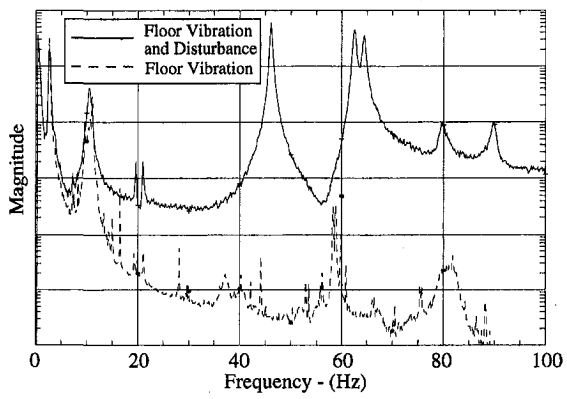

Fig. 4 Autospectra with and without artificial disturbance

The CMIF's, which are used extensively in robust control design, are the singular values of the FRF matrix as a function of frequency. The peaks of the CMIF occur at the same frequencies as the system resonances. Multiplicity of roots is indicated by peaks in the secondary and tertiary CMIF's; therefore, the system order can be determined simply by counting the peaks in the CMIF's over the bandwidth of interest. Because of the first order form of the extracted model, the system order is twice the number of peaks in the CMIF's.

In performing ERADC analysis the correlation matrix size is selected to be significantly larger than the estimated system order to account for noise, nonlinearities, etc. System order, length of time records, and matrix size are varied and convergence of parameters is observed. In particular, the eigenvalues of the system should correspond to the peaks in the CMIF, and the damping ratio values should stabilize with increasing matrix size, system order and length of time record. As a single figure of merit to determine the accuracy of a derived model, CMIF's of the measured FRFs and analytical FRFs, calculated from the realized model, can be compared.

System models were estimated in using the ERADC algorithm as coded in the NASA System Identification toolbox (Juang, 1991). The model was estimated over the frequency range of 0 to 200 Hz. Additional analyses were performed for higher resolution/signal-to-noise analysis band of 0 to 25 Hz. Shown in Fig. 5 is a comparison of the CMIF's for the measured and analytical FRF's calculated from the experimentally derived model. The CMIF's are in excellent agreement up to approximately 150 Hz. Above 150 Hz the modal density of the structure is extremely high principally due to local modes of the individual struts. Additionally, the "rigid-body" modes, less than 5 Hz, are not well characterized. The principal reason is that contribution of these modes to the response matrix is a result of external unmeasured inputs and not related to system inputs. These modes are marginally observable and controllable and are poorly characterized by the all of the system identification techniques employed.

The full order system model contained 54 states. Because of instrumentation problems, the final system model consisted of seven inputs (four control actuators and three disturbances) and ten outputs (three performance measures and seven feedback sensors). The dynamics of the truss consist of lightly damped ($\sim$0.5 percent) modes up to ($\sim$120 Hz). The structure has a discrete modal nature up to $\sim$150 Hz. Above 150 Hz the dynamics become very dense and dominated by many localized modes of the truss. The suspension modes of the isolation mass are at low frequency ($\sim$1–3 Hz). The low frequency range also has poor signal to noise characteristics due to the ambient floor vibration.

4 Control Design Methods

In this section, frequency weighted LQG and Maximum Entropy will be reviewed. As a prelude to the discussion of fre-

quency weighted LQG, LQG with cross weighting terms will be reviewed to establish definitions and nomenclature. Only the main results of LQG will be stated, more complete details can be found in Maciejowski (1989).

4.1 LQG Theory. The problem addressed by LQG theory is the following. Given a system and associated model, Fig. 6 and Eq. (1), respectively, design a compensator of the form shown in Eq. (2), where u, v, w, x, x_c, y, z are the control signal, sensor noise, disturbance, system state, compensator state, performance and sensor vectors, respectively.

$$\begin{aligned} \dot{x} &= \mathbf{A}x + \mathbf{B}_u u + \mathbf{B}_w w \\ y &= \mathbf{C}x + \mathbf{D}_u u + \mathbf{D}_w w \qquad \text{:System Dynamics—}G_0 \\ z &= \mathbf{M}x + \mathbf{N}_u u + \mathbf{N}_w w + v \end{aligned} \tag{1}$$

$$\begin{aligned} \dot{x}_c &= \mathbf{A}_c x_c + \mathbf{B}_c z \\ u &= \mathbf{C}_c x_c \end{aligned} \qquad \text{:Compensator—}K \tag{2}$$

The signals w and v are white zero-mean gaussian stochastic processes which have the following covariances $E\{ww^T\} = \mathbf{V}_1 \geq 0 \quad E\{vv^T\} = \mathbf{V}_2 > 0 \quad E\{wv^T\} = \mathbf{V}_{12}$. The problem is to find a control law which minimizes the cost function shown in Eq. 3, where $\mathbf{R}_1 = \mathbf{R}_1^T \geq 0$, $\mathbf{R}_2 = \mathbf{R}_2^T > 0$, and $\mathbf{R}_{12}$ are weighting matrices.

$$J = \lim_{T\to\infty} E\left\{ \int_0^T (x^T\mathbf{R}_1 x + u^T\mathbf{R}_2 u + 2y^T\mathbf{R}_{12}u)dt \right\} \tag{3}$$

The solution to the LQG problem is prescribed by the separation principle, which solves the problem in two uncoupled steps.

- Obtain an optimal estimate, $\hat{x}$, of the state x such that $E\{(x - \hat{x})^T(x - \hat{x})\}$ is minimized. The solution to this problem is given by Kalman filter theory (LQE).
- Use the state estimate, $\hat{x}$, as if it were an exact measurement of the state to solve the deterministic linear quadratic regulator (LQR) problem.

The solution to the LQE and LQR problems each involve the solution of an algebraic Riccati equation. The Kalman-filter gain matrix F is given by Eq. (4) in which $\mathbf{Q}$ is the solution of the Riccati Eq. (5), where $\bar{\mathbf{A}} = \mathbf{A} - \mathbf{B}_w\mathbf{V}_{12}\mathbf{V}_2^{-1}\mathbf{M}$ and $\bar{\mathbf{V}}_1 = \mathbf{V}_1 - \mathbf{V}_{12}\mathbf{V}_2^{-1}\mathbf{V}_{12}^T$.

$$\mathbf{F} = (\mathbf{B}_w\mathbf{V}_{12} + \mathbf{Q}\mathbf{M}^T)\mathbf{V}_2^{-1} \quad \text{:LQE Gain} \tag{4}$$

$$\mathbf{Q}\bar{\mathbf{A}}^T + \bar{\mathbf{A}}\mathbf{Q} - \mathbf{Q}\mathbf{M}^T\mathbf{V}_2^{-1}\mathbf{M}\mathbf{Q} + \mathbf{B}_w\bar{\mathbf{V}}_1\mathbf{B}_w^T = 0 \qquad \text{:LQE Riccati} \tag{5}$$

The optimal state feedback matrix, G, of the LQR problem is given by Eqs. (6) and (7), where, $\tilde{\mathbf{A}} = \mathbf{A} - \mathbf{B}_u\mathbf{R}_2^{-1}\mathbf{R}_{12}^T$ and $\tilde{\mathbf{R}}_1 = \mathbf{R}_1 - \mathbf{R}_{12}\mathbf{R}_2^{-1}\mathbf{R}_{12}^T$.

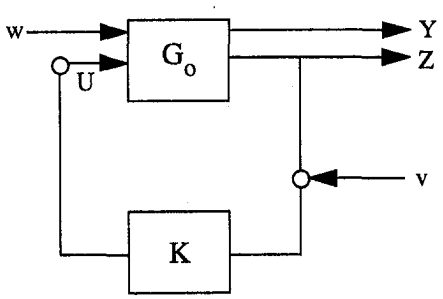

Fig. 6 System schematic

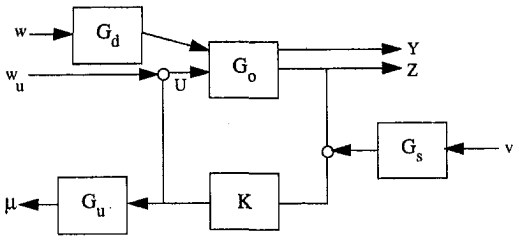

Fig. 7 Frequency weighted system schematic

$$\mathbf{G} = -\mathbf{R}_2^{-1}(\mathbf{R}_{12}^T + \mathbf{B}_u^T\mathbf{P}) \quad \text{:LQR Gain} \tag{6}$$

$$\tilde{\mathbf{A}}^T\mathbf{P} + \mathbf{P}\tilde{\mathbf{A}} - \mathbf{P}\mathbf{B}_u\mathbf{R}_2^{-1}\mathbf{B}_u^T\mathbf{P} + \tilde{\mathbf{R}}_1 = 0 \quad \text{:LQR Riccati} \tag{7}$$

The matrices for the compensator designed by the LQG procedure which is of the form shown in Eq. (2) are given in Eq. (8).

$$\begin{aligned} \mathbf{A}_c &= \mathbf{A} + \mathbf{B}_u\mathbf{G} - \mathbf{F}(\mathbf{M} + \mathbf{N}_u\mathbf{G}) \\ \mathbf{B}_c &= \mathbf{F}\mathbf{M} \\ \mathbf{C}_c &= \mathbf{G} \end{aligned} \tag{8}$$

The LQG development is based on optimization methods with a specified model form. The closed loop system behaves well under the following conditions

- The model is valid for all values of inputs and states and the dynamics are well described at all frequencies.
- The Kalman filter design also assumes that the dynamics are known equally well at all frequencies. This may also make combination of the Kalman filter and the LQR control law extremely sensitive to errors.
- The optimality of the Kalman filter is strongly dependent on the accuracy of the noise statistics.

The experience with LQG controllers designed with white noises have not been completely satisfactory (Doyle, 1978). There are no explicit ways in the technique presented above to design a controller with a specified bandwidth or stability margins.

4.2 Frequency Weighted LQG Theory. An effort to correct some of the problems associated with LQG theory have been implemented through the use of colored noises and frequency dependent weighting in LQG formulation. Gupta (1980) presented a method of incorporating frequency dependent cost functions into basic LQG theory. A formulation for Frequency Weighted LQG (FWLQG) which incorporates the methods presented in references Gupta (1980), Safonov (1981) and Opdenacker et al. (1990) is presented here.

Figure 7 shows a schematic of a system which has a control signal weighting filter, G_u and noise coloring filters G_d and G_s appended. G_0 and K are as defined previously. The state space matrices corresponding to the weighting and coloring filters are defined below.

$$G_u\text{—Control Weighting Filter: } \begin{bmatrix} \mathbf{A}_\mu & \mathbf{B}_\mu \\ \mathbf{C}_\mu & \mathbf{D}_\mu \end{bmatrix}$$

$$G_s\text{—Sensor Noise Coloring Filter: } \begin{bmatrix} \mathbf{A}_s & \mathbf{B}_s \\ \mathbf{C}_s & \mathbf{D}_s \end{bmatrix}$$

$$G_d\text{—Disturbance Noise Coloring Filter: } \begin{bmatrix} \mathbf{A}_d & \mathbf{B}_d \\ \mathbf{C}_d & \mathbf{D}_d \end{bmatrix}$$

The rationale behind the definition of inputs and weightings are as follows.

- The external disturbance that the control system is to reject is the white noise disturbance w colored by G_d.
- The white noise disturbance w_u is used to enhance stability margin at the input. The intensity of this noise can be physically interpreted as uncertainty in the actuator.
- The measurement noise v is colored by G_s to simulate physical sensor noise or possible model uncertainty.
- The filtered control signal, μ, can be used to penalize control effort outside the frequency range of interest.

The augmented system equations are shown below. The outputs in Eq. (10), Y and μ are the performances to be minimized and frequency weighted control signal respectively, which are in the cost function for FWLQG, Eq. (12). The signals w, w_u, and v are white zero-mean gaussian stochastic process with

$$E\{ww^T\} = \mathbf{W} \geq 0 \quad E\{w_u w_u^T\} = \mathbf{U} \geq 0 \quad E\{vv^T\} = \mathbf{V} > 0$$

$$\begin{bmatrix} \dot{x} \\ \dot{x}_d \\ \dot{x}_s \\ \dot{x}_\mu \end{bmatrix} = \begin{bmatrix} \mathbf{A} & \mathbf{B_w C_d} & \mathbf{0} & \mathbf{0} \\ \mathbf{0} & \mathbf{A_d} & \mathbf{0} & \mathbf{0} \\ \mathbf{0} & \mathbf{0} & \mathbf{A_s} & \mathbf{0} \\ \mathbf{0} & \mathbf{0} & \mathbf{0} & \mathbf{A}_\mu \end{bmatrix} \begin{bmatrix} x \\ x_d \\ x_s \\ x_\mu \end{bmatrix} + \begin{bmatrix} \mathbf{B_u} \\ \mathbf{0} \\ \mathbf{0} \\ \mathbf{B}_\mu \end{bmatrix} u + \begin{bmatrix} \mathbf{B_w D_d} & \mathbf{B_u} & \mathbf{0} \\ \mathbf{B_d} & \mathbf{0} & \mathbf{0} \\ \mathbf{0} & \mathbf{0} & \mathbf{B_s} \\ \mathbf{0} & \mathbf{0} & \mathbf{0} \end{bmatrix} \begin{bmatrix} w \\ w_u \\ v \end{bmatrix} \quad (9)$$

$$\begin{bmatrix} \mathbf{Y} \\ \mu \end{bmatrix} = \begin{bmatrix} \mathbf{C} & \mathbf{0} & \mathbf{0} & \mathbf{0} \\ \mathbf{0} & \mathbf{0} & \mathbf{0} & \mathbf{C}_\mu \end{bmatrix} \begin{bmatrix} x \\ x_d \\ x_s \\ x_\mu \end{bmatrix} + \begin{bmatrix} \mathbf{D_u} \\ \mathbf{D}_\mu \end{bmatrix} u + \begin{bmatrix} \mathbf{D_w} & \mathbf{0} & \mathbf{0} \\ \mathbf{0} & \mathbf{0} & \mathbf{0} \end{bmatrix} \begin{bmatrix} w \\ w_u \\ v \end{bmatrix} \quad (10)$$

$$Z = [\mathbf{M} \quad \mathbf{0} \quad \mathbf{C_s} \quad \mathbf{0}] \begin{bmatrix} x \\ x_d \\ x_s \\ x_\mu \end{bmatrix} + [\mathbf{N_u}] u + [\mathbf{N_w} \quad \mathbf{N_u} \quad \mathbf{D_s}] \begin{bmatrix} w \\ w_u \\ v \end{bmatrix} \quad (11)$$

For this design method the cost function to be minimized is shown in Eq. (12). The two terms that are included in the cost function are y (the performance to be minimized) and μ (the frequency weighted control signal). Where $Q = Q^T \geq 0$ and $\mathbf{R} = \mathbf{R}^T > 0$ are weighting matrices.

$$J = \lim_{T \to \infty} E\left\{ \int_0^T (y^T \mathbf{Q} y + \mu^T \mathbf{R} \mu) dt \right\} \quad (12)$$

The augmented system matrices and the following weighting matrices can be used with the basic LQG solution shown previously.

$$\mathbf{R}_1 = \begin{bmatrix} \mathbf{C}^T\mathbf{Q}\mathbf{C} & \mathbf{0} & \mathbf{0} & \mathbf{0} \\ \mathbf{0} & \mathbf{0} & \mathbf{0} & \mathbf{0} \\ \mathbf{0} & \mathbf{0} & \mathbf{0} & \mathbf{0} \\ \mathbf{0} & \mathbf{0} & \mathbf{0} & \mathbf{C}_\mu^T \mathbf{R} \mathbf{C}_\mu \end{bmatrix}$$

$$\mathbf{R}_2 = \mathbf{D}_\mu^T \mathbf{R} \mathbf{D}_\mu \quad \mathbf{R}_{12} = \begin{bmatrix} \mathbf{C}^T\mathbf{Q}\mathbf{D_u} \\ \mathbf{0} \\ \mathbf{0} \\ \mathbf{C}_\mu^T \mathbf{R} \mathbf{D}_\mu \end{bmatrix} \quad (13)$$

$$\mathbf{V}_1 = \begin{bmatrix} \mathbf{W} & \mathbf{0} & \mathbf{0} \\ \mathbf{0} & \mathbf{U} & \mathbf{0} \\ \mathbf{0} & \mathbf{0} & \mathbf{V} \end{bmatrix} \quad \mathbf{v}_2 = [\mathbf{V}] \quad \mathbf{V}_{12} = \begin{bmatrix} \mathbf{0} \\ \mathbf{0} \\ \mathbf{V} \end{bmatrix} \quad (14)$$

4.3 Maximum Entropy. Maximum entropy permits the design of robust controllers with respect to structured parametric uncertainty to be determined by the quadratic cost functional. Given a nominal linear system modeled in state space form (e.g., $\mathbf{A_0}$, $\mathbf{B_0}$, $\mathbf{C_0}$, $\mathbf{D_0}$), the parametric uncertainty can be modeled with a set of parameter uncertainty matrices (e.g., $\Delta\mathbf{A}$, $\Delta\mathbf{C}$, $\Delta\mathbf{M}$, ... etc.). For example, assuming the parametric error is associated with modal frequency or damping, the only parametric error matrices necessary are for A (i.e., ΔA); however, if these errors are independent or arise from different sources, parametric error matrices can be defined for each source of uncertainty, $\Delta\mathbf{A_i}$. The uncertain dynamics of the system can be expressed as shown in Eq. 15, where $\alpha_i(t)$ is a zero-mean multiplicative white noise process with n uncorrelated error sources.

$$\mathbf{A} = \mathbf{A_0} + \sum_{i=1}^{n} \alpha_i(t) \Delta \mathbf{A_i} \quad (15)$$

With the addition of the multiplicative white noise, the first order state space form of the system dynamics, Eq. (1), become as shown in Eq. (16).

$$\dot{x} = (\mathbf{A}_0 + \sum_{i=1}^{n} \alpha_i(t) \Delta \mathbf{A_i}) x + \mathbf{B_u} u + \mathbf{B_w} w \quad (16)$$

Once the system dynamics are represented with stochastic differential equations, as shown in Eqs. (17) and (18) the necessary conditions for optimality can be derived (Bernstein and Greeley, 1986). The resulting necessary conditions take the form of two Riccati equations and two Lyapunov equations, coupled by the stochastic parameters. The separation principle which is a foundation of LQG design is invalid in the presence of the parametric uncertainty expressed by maximum entropy.

$$dx = (\mathbf{A_S} dt + \sum_{i=1}^{n} d\alpha_i(t)) x + \mathbf{B_u} u + \mathbf{B_w} w \quad (17)$$

$$\mathbf{A_S} = \mathbf{A}_0 + \tfrac{1}{2} \sum_{i=1}^{n} \Delta \mathbf{A_i} \quad (18)$$

The coupled set of two Riccati and two Lyapunov equations can be solved using homotopy methods. Homotopy methods are used to solve problems of the form: Given sets Θ and Φ contained in $\Re^n$ and a mapping F: $\Theta \Rightarrow \Phi$, find solutions to $F(\Theta) = 0$. Homotopy methods embed $F(\Theta) = 0$ in larger problem $H(\Theta(\lambda), \lambda) = 0$ for $\lambda \epsilon [0, 1]$, in which $H(\Theta(1), 1) = F(\Theta)$ and $H(\Theta(0), 0) = 0$. The homotopy method is an algorithm to compute the curve $(\Theta(\lambda), \lambda)$ such that a known initial solution $\Theta(0)$ is transformed to a desired solution $\Theta(1)$ which satisfies $F(\Theta(1)) = 0$. A Matlab toolbox (Collins et al., 1994) has been developed to implement the homotopy solution methods for Maximum Entropy robust control design of LQG controllers.

5 Sandia Truss Experimental Control Implementation

5.1 Control Design Modelling and Analysis. The model of the Sandia Truss used for control design was a 32 state truncated version of the 54 state ERADC model described in Section 3 in which the very uncertain high frequency dynamics above 150 Hz have been truncated. Figure 8 shows a comparison of the actuator—sensor channels for the two models. The low frequency dynamics of the suspension were retained in the control design model even though they are very uncertain and are in a region of low SNR.

The structured singular value, μ, was used in the control design process to analytically evaluate the robust stability of different control designs. Maciejowski (1989) provides a brief overview of the structured singular value, μ, and its properties.

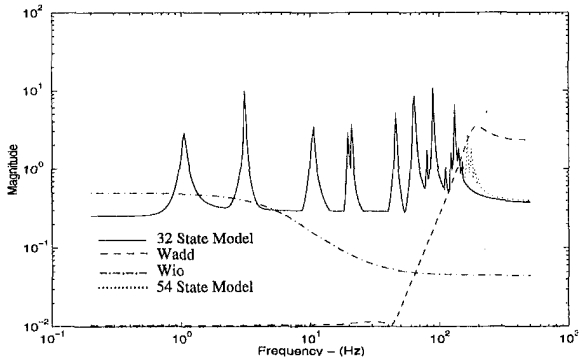

Fig. 8 Maximum singular value of the actuator—sensor channels of the 54 state and the 32 state control design model

In the definition of μ, there is an underlying structure, Δ, which for robust stability analysis depends on the uncertainty model of the system. The uncertainty model of the system, Δ, is in a feedback loop with the system dynamics, G_0, and may have structure which correspond to different forms of uncertainty (i.e. additive uncertainty due to unmodelled dynamics or multiplicative uncertainty in the modeshapes at the sensor or actuators, etc.). Robust stability is achieved if stability is guaranteed for all allowable Δ's. Alternatively, the H_∞ norm could be used via the small gain theorem as a measure of robust stability; however, if Δ has structure this approach can be quite conservative. The structured singular value, μ, takes the structure of the perturbation into account and provides a less conservative measure of robust stability. The structured singular value which is a matrix function is defined for a complex matrix, $\mathbf{M} \epsilon \mathbf{C}^{nxn}$ by Eq. (19). The stability boundary is at $\mu = 1$.

$$\mu(\mathbf{M}) \equiv \frac{1}{\min \{\bar{\sigma}(\Delta) : (\det (\mathbf{I} - \mathbf{M}\Delta) = 0)\}} \qquad (19)$$

The uncertainty model, Δ, used in the robust stability analysis of the Sandia Truss consisted of three blocks: additive uncertainty, input, and output multiplicative uncertainty. The additive uncertainty weight, Wadd, which is shown in Fig. 8, envelops the unmodelled dynamics of the system. The input and output multiplicative uncertainty, W_{io}, was modeled as a frequency dependent weight with 50 percent uncertainty for frequencies <3 Hz and 5 percent uncertainty for high frequency as shown in Fig. 8. Therefore, the uncertainty model, Δ, used in the robust stability analysis has structure; and, Δ consists of 3 blocks (i.e. additive uncertainty, input multiplicative, output multiplicative).

5.2 Frequency Weighted LQG (FWLQG) Controllers. A series of FWLQG controllers of increasing control authority were designed for the initial phase of the study. The purpose of this series of designs were to find the limits of system stability and performance. The control signal weight, G_u, was a diagonal 4-input/4-output, 48 state frequency dependent matrix which is appended to the control design model. The diagonal entries in the control signal weight, G_u, was a band-stop butterworth filter shown in Fig. 9. The high frequency break point of G_u was chosen to gain stabilize the high frequency unmodelled dynamics of the system (>150 Hz). G_u was shaped to reduce the system loop gain rapidly in the frequency range 120–150 Hz while the system dynamics are still discrete and reasonably well modelled. The low frequency break point was chosen to stabilize the poorly characterized suspension modes and prevent the propagation of noise in the control loop due to the poor SNR in the low frequency range (<10 Hz). Previous control design studies on this system indicated that coloring of disturbance, G_d, and sensor, G_s, noises was difficult to use in addressing uncertainty without significant loss of system performance. Therefore, the disturbance, w, and actuator, w_u, noises were white with covariances of 3 and 0.5. The sensor noise, v, was chosen to have a covariance 0.01 of the sensor covariance due to w and w_u.

Table 1 Frequency weighted LQG design summary

	Design Information			Robust Stability - μ		Comments	
Name	W_u	Q	ME	K_{80}	K_{32}	K stability	System stability[3]
nom1	note 1	Q*1	none	0.47	0.48	stable	stable
nom2	note 1	Q*2	none	0.87	0.92	stable	unstable
nom24	note 1	Q*2.4	none	1.08	1.09	stable	unstable
nom27	note 1	Q*2.7	none	1.13	1.10	unstable	
nom27me2	note 1	Q*2.7	note 2	0.58	0.63	stable	stable

note 1: See Figure 9.
note 2: 2% frequency uncertainty in 10-150 Hz modes.
note 3: experimental assessment of stability

Table 1 summarizes the four frequency weighted LQG designs (Nom1, Nom2, Nom24, Nom27) with increasing control authority which are denoted in table 1 by multiplication of the state weighting matrix, Q, by a scalar of increasing magnitude (e.g. Q*2). The robust stability μ for these designs are shown in the table. Reduced order 32 state controllers suitable for implementation were obtained by a balanced truncation of the 80 state full order controller, (Moore, 1981). The response of the 120 Hz mode was most affected by controller reduction.

The design Nom1 yielded a stable compensator, K, which also produced a stable closed loop system on experimental implementation. As control authority was increased, the closed loop system was unstable experimentally. The highest authority controller, Nom27, also had an unstable compensator, K.

Figure 10 shows that robust stability degrades (i.e., μ increases) as control authority is increased for the FWLQG designs. μ for the Nom1 controller is well below 1 at all frequencies; however, μ for the Nom27 controller is >1 for two frequencies in the controller bandwidth, which indicates that the

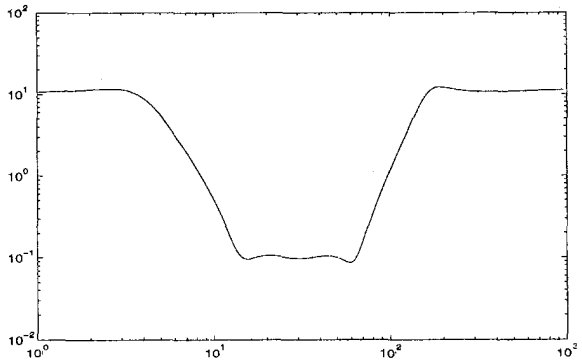

Fig. 9 Control signal frequency dependent weighting, G_u

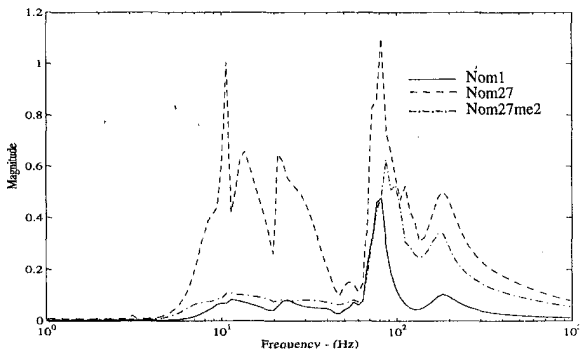

Fig. 10 Robust stability μ for 32 state LQG controllers using frequency weighting and maximum entropy

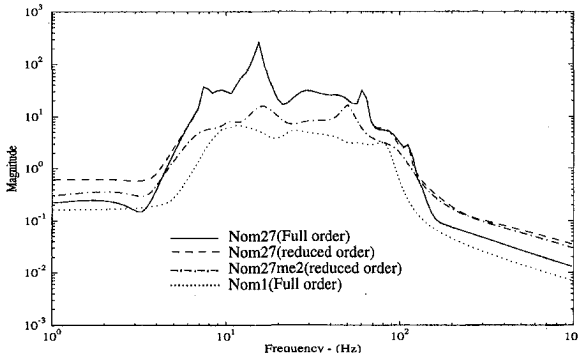

Fig. 11 Maximum singular value plots for LQG controllers, K, using frequency weighting and maximum entropy

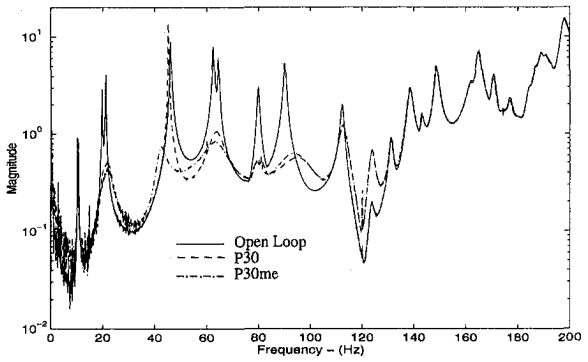

Fig. 13 Comparison of FWLQG and FWLQG/ME experimental closed-loop performance with a perturbed control design model

boundary of stability has been crossed. Figure 11 shows a maximum singular value plot for several of the controllers, K, discussed. This figure shows that controller reduction of Nom27 reduced the roll-off at low and high frequency with little effect in the control bandwidth. Due to the nature of the frequency weights used in the FWLQG designs, the controllers have a bandpass nature.

5.3 Frequency Weighted LQG With Maximum Entropy (FWLQG/ME) Designs. Several formulations of maximum entropy were studied and designed; however, the controller reported here is Nom27me2. This controller used the same control signal frequency dependent weighting and authority as Nom27; however, frequency uncertainty for the in-band modes from 10 to 120 Hz was incorporated in the ME design. The FWLQG/ME controllers were calculated with homotopy algorithms using the FWLQG designs with no uncertainty for the in-band dynamics as the starting point. The ME controller Nom27me2 is stable; and, the closed loop system was stable with better performance than Nom1. Maximum entropy produced a more robust and stable controller than the FWLQG controller without ME.

Also, ME had the effect of lowering the in-band gain, reduced the roll-off rate at low and high frequency, and produced a stable controller as well as a stable system. Analytically Nom27me2 also has better robust stability properties than Nom27, Fig. 10. The gain of Nom27me2 is greater than Nom1 and produced significantly better performance. Figure 12 shows the closed loop experimental performance for the Nom1 and Nom27me2 controllers.

5.4 Structured Uncertainty Experiment. In order to experimentally study the effect of maximum entropy on structured uncertainties, the frequency of the 45.9 Hz mode in the control design model was perturbed. This produced a mismatch in the system dynamics at 45.9 Hz between the model used to perform

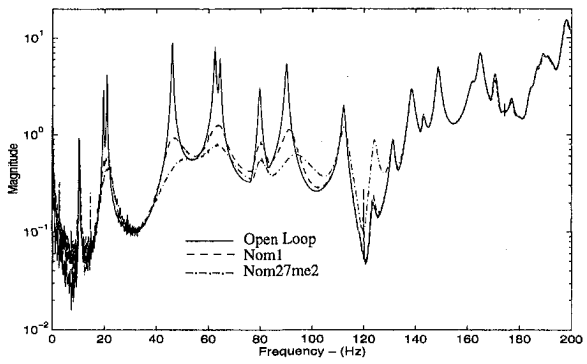

Fig. 12 Disturbance-performance maximum singular value plots for LQG controllers using frequency weighting and maximum entropy

control design and the actual system dynamics. Then a FWLQG controller was designed using the same weighting's as the Nom27 controller which was analytically stable. The magnitude of the frequency perturbation was increased until the closed loop system was unstable.

Figure 13 shows the experimental closed loop performance for the FWLQG controller (P30) with the maximum frequency perturbation which still produced an experimentally stable closed loop system. Figure 13 shows that the 45.9 Hz mode is destabilized.

Now a FWLQG/ME controller (P30me) was designed which incorporated frequency uncertainty for the 45.9 Hz mode into the control design. Figure 13 shows the experimental closed loop performance for the FWLQG/ME controller, which stabilized the 45.9 Hz mode and improved system performance.

6 Summary and Conclusions

This study evaluated the abilities of system identification using the eigensystem realization algorithm with data correlation (ERADC) and control design using frequency weighted LQG (FWLQG) and maximum entropy (ME).

A full order (54 state) control design model was identified using ERADC. The control design model was quite accurate in the frequency range of 10–150 Hz. However, above 150 Hz the system dynamics became quite dense due to localized dynamics of the truss. Below 10 Hz the dynamics were poorly identified due to significant unmeasured disturbances during the measurement of the system frequency response functions.

FWLQG was shown to be capable of control design with a specified bandwidth and gain stabilization of additive uncertainty due to unmodeled dynamics. However, FWLQG was shown to be sensitive to structured uncertainty of in-band system dynamics. Maximum entropy provided increased robustness properties for the controller. Maximum entropy reduced the gain and roll-off rate of the controller as well as producing a high performance stabilizing controller. An experimental demonstration of the ability of maximum entropy to stabilize a structured (frequency) uncertainty in the system dynamics was performed.

In order to achieve specified constraints, the LQG method with frequency weighting and maximum entropy is not explicit and requires iterative design. Homotopy methods were necessary to calculate the maximum entropy controllers; however the computational burden was not prohibitive.

Acknowledgments

This work was performed at Sandia National Laboratories and was supported by the U.S. Department of Energy under Contract Number DE-AC04-94AL85000 via the Laboratory Directed Research and Development program. The authors would like to thank the reviewers for their helpful comments.

References

Allen, J. J., Lauffer, J. P., Marek, E. L., 1990, "The Sandia Structural Control Experiments," *Proceedings of the First Joint U.S./Japan Conference on Adaptive Structures,* Maui, HI, Nov.

Bendat, J. S., and Piersol, A. G., 1986, *Random Data,* Wiley-Interscience, New York.

Bernstein, D. S., and Greeley, S. W., 1986, "Robust Controller Synthesis Using the Maximum Entropy Design Equations," *IEEE Transactions on Automatic Control,* Vol. AC-31, Apr., pp. 362–364.

Collins, E. G., Jr., Phillips, D. J., and Hyland, D. C., 1991, "Robust Decentralized Control Laws for the ACES Structure," *IEEE Control Systems,* Apr., pp. 62–70.

Collins, E. G., Davis, L. D., Richter, S., 1994, "Homotopy Algorithms for Maximum Entropy Design," *Journal of Guidance, Control and Dynamics,* Vol. 17, No. 2, Mar.–Apr., pp. 311–321.

Collins, E. G., King, J. A., Phillips, D. J., and Hyland, D. C., 1992, "High Performance, Accelerometer-Based Control of the Mini-MAST Structure," *Journal of Guidance, Control and Dynamics,* Vol. 15, No. 4, July–Aug., pp. 885–892.

Doyle, J. C., "Guaranteed Margins for LQG regulators," 1978, *IEEE Transactions on Automatic Control,* Vol. AC-23, No. 4, Aug., pp. 756–757.

Gupta, N. K., 1980, "Frequency-Shaped Cost Functionals: Extension of Linear-Quadratic-Gaussian Design Methods," *J. Guidance, Control and Dynamics,* Vol. 3, No. 6, Nov.–Dec.

Hyland, D. C., Junkins, J. L., Longman, R. W., 1993, "Active Control Technology for Large Space Structures," *Journal of Guidance, Control and Dynamics,* Vol. 16, No. 5, Sept.–Oct.

Juang, J. N., Cooper, J. E., and Wright, J. R., 1988, "An Eigensystem Realization Algorithm Using Data Correlations (ERA/DC) for Modal Parameter Identification," *Journal of Control Theory and Advanced Technology,* Vol. 4, No. 1, Mar., pp. 5–14.

Juang, J. N., Horta, L. G., Phan, M. Lew, J. S. Chen, C. W., 1991, "Observer/System Realization ToolBox," NASA Langley Research Center, Aug. 21.

Maciejowski, J. M., 1989, *Multivariable Feedback Design,* Addison-Wesley.

Moore, B., 1981, "Principal Component Analysis in Linear Systems: Controllability, Observability, and Model Reduction," *EEE Trans. Automat. Contr.,* AC-26, Feb.

Opdenacker, Ph. C., et al., 1990, "Reduced-Order Compensator Design for a Flexible Structure," *J. Guidance and Control,* Vol. 13, No. 1, Jan.–Feb.

Rocklin, G., Crowley, J., Vold, H., 1985, "A Comparison of H1, H2, and Hv Frequency Response Function," *Proceedings of the 3rd International Modal Analysis Conference,* Orlando, Florida, Jan.

Safonov, M. G., 1981, "Feedback Properties of Multivariable Systems: The Role and Use of the Return Difference Matrix," *IEEE Trans. Automat. Contr.,* AC-26, no. 1, Feb., pp. 47–65.

Shih, C. Y., Tsuei, Y. G., Allemang, R. J., and Brown, D. I., 1989, "Complex Mode Indication Function and its Applications," *Proceedings of the 7th International Modal Analysis Conference,* Las Vegas, Nevada, pp. 533–540.